

# Non-Commutative fluid: an alternative source of cosmic acceleration

Arpan Krishna Mitra<sup>1,\*</sup> and Raj Kumar Das<sup>2,†</sup>

<sup>1</sup>*Aryabhatta Research Institute of Observational Sciences (ARIES), Nainital 263001, India*

<sup>2</sup>*Physics and Applied Mathematics Unit, Indian Statistical Institute, 203 B. T. Road, Kolkata 700108, India*

We have developed a Hubble function based on Newtonian Cosmology using non-commutative fluid equations. Our Hubble function contains cosmic fluids with the signature of a new cosmological parameter  $\sigma$ , motivated by a non-commutative Poisson bracket structure. Interestingly, this Hubble function does not include any external fluid content related to dark energy or the Cosmological constant; the parameter  $\sigma$  acts as the source of accelerated expansion. In this work, we aim to explain the phenomenon of the accelerating expansion of the universe without "dark energy". Additionally, we have verified the observational bounds for  $\sigma$  to assess its potential in explaining the accelerated expansion.

## I. INTRODUCTION

The experiments that involved type Ia supernovae (SNe Ia) data strongly suggest a late-time acceleration of the universe[1, 2]. Current data dictates the existence of a Friedman-Lemaître cosmology with zero curvature, CDM along with baryons as their dominant components in the matter sector at present and a cosmological constant  $\Lambda$ . In the early phase both matter and radiation were dominant, causing the deceleration in the expansion of the universe. The vacuum energy [3] got its dominance more recently, leading to this late-time acceleration. While the incorporation of the cosmological constant provides the simplest explanation of this late-time acceleration, any attempt of theoretical calculation of this constant has failed miserably. For this reason, the  $\Lambda$ CDM model is considered a well-established vanilla model to explain cosmic acceleration and large-scale structure of the universe. However, the model has some serious issues, including tension anomalies[4–10], the coincidence problem[11], and the cosmological constant problem[12], among others. These issues are the key motivation for the development of alternative cosmological models that address these drawbacks. A plethora of models have been proposed, approaching the problem from different perspectives, including phenomenological models and extended theoretical explanations such as Modified Gravity, Scalar Field Models or any other non-standard theories.

In general, the  $\Lambda$ CDM model consists of two components, a "Cosmological Constant" ( $\Lambda$ ) playing the role of "Dark Energy" and the "Cold Dark Matter" (CDM), where the term "cold" refers to the non-relativistic nature of dark matter. As mentioned previously, several alternative proposals try to explain the accelerating expansion phase. "Matter Creation Cosmology" is one of the recent theories among them [13–19].

The concept of matter creation deals with creation of cold dark matter(CCDM) due to gravitationally induced particle(non-relativistic species) production. This particle production may cause to the required negative pressure so it can be an alternative to "Dark Energy". This behavior of driving the cosmic acceleration through particle production phenomena has also been presented in [20]. In the matter creation scenario, there is no need for a cosmological constant or any quintessence-type component. There are several perspectives on how to outline the concept of matter creation. In this work, we have approached matter creation through a noncommutatively corrected fluid term in Newtonian cosmology.

Noncommutative (NC) spacetime effects in ideal fluid dynamics is an area that has experienced some recent interest[21–24]. In an earlier work [25], we have dealt with our extended NC fluid variable algebra and a subsequent study of the generalized continuity and conservation equations. We provided an outline of the effects on cosmological principles induced by the NC-modified fluid dynamics.

By implementing the extended NC fluid dynamic equations, we have derived a modified Friedmann equation (FE) in which the extended NC fluid affects the matter sector and generates an effective curvature component. When the extended NC terms vanish, the FE simplifies to a non-interacting matter-curvature scenario. No additional effective cosmological constant arises. Instead, it modifies the matter and curvature components, influencing their individual equations of state. In this way, we have established a connection between extended NC fluids and the matter creation scenario.

This paper is organized as follows: in section-II, we have discussed the theoretical foundation of our model, the background cosmic flow dynamics. The effects of NC extension are explained in section-III. The details of the dataset used for our analysis are provided in section-IV. The observational constraints regarding our model are discussed in section-V. Additionally, a brief discussion on the statistical comparison of fitting criteria is presented in section-VI. Finally, in section-VII, we summarize and discuss about the future extension of our work.

<sup>1</sup> Author of correspondence: raj1996cool@gmail.com

\* arpankmitra@gmail.com; arpankmitra@aries.res.in

† raj1996cool@gmail.com

## II. FRIEDMANN EQUATION MOTIVATED FROM NON-COMMUTATIVE COSMOLOGY

The very first step to deal with NC fluid is the scheme one follows to introduce the NC effect in the fluid dynamic equations. We have two distinct routes for this purpose: (i) to apply the (Groenwald-Moyal)  $\star$ -product directly in the Eulerian field theory of fluid to introduce NC contributions. (ii) To introduce NC algebra in Lagrangian (discrete) fluid degrees of freedom, which subsequently percolates to the Euler (field) fluid degrees of freedom. We have followed the second path as NC generalisation can be unambiguously done for discrete variables. The ideal fluid dynamic equations get modified on the introduction of NC (Non-Commutative) effects. We already have the NC-corrected fluid dynamic equations and corresponding cosmological Friedman equation [25].

The explicit form of Friedman acceleration Equation with NC corrected term is given by,

$$\frac{\ddot{a}}{a} + \frac{4\pi G\rho_0}{3} + \sigma H^2 = 0 \quad (1)$$

Here,  $\rho_0$  is the background density of the matter sector of the cosmic fluid, the last term of the equation  $\sigma H^2$  represents the noncommutative (NC) correction. Here,  $\sigma = \delta_{ij}\sigma_{ij}$ , where  $\sigma_{ij}$  an NC parameter introduced in the Poisson bracket of the position and momentum variable, subsequently breaking the inherent symmetry[25]. The background matter fluid  $\rho_0$  follows the continuity equation, which incorporates the NC-corrected equation of state, as shown in the expression:

$$\dot{\rho}_0 + H(3 + \sigma)\rho_0 = 0 \implies \rho_0 = \bar{\rho}_0 a^{-(3+\sigma)} \quad (2)$$

where,  $\bar{\rho}_0$  is the present-day background matter density. On replacing the acceleration term as  $\frac{\ddot{a}}{a} = \dot{H} + H^2$  in (1) we get,

$$\frac{dH}{dt} + H^2(1 + \sigma) + \frac{4\pi G\rho_0}{3} = 0. \quad (3)$$

With  $\dot{a} = aH$ , (3) becomes,

$$\frac{dH^2}{da} + H^2 \frac{2(1 + \sigma)}{a} = -\frac{8\pi G}{3}\rho_0. \quad (4)$$

Exploiting the concept of integrating factor, we arrive at the equation

$$\frac{d}{da} \left[ H^2 a^{2(1+\sigma)} \right] = -\frac{8\pi G}{3} a^{2(1+\sigma)} \rho_0. \quad (5)$$

Combined with the NC extended continuity equation (2), (4) produces the cherished expression of the Hubble function

$$H^2 = H_0^2 \left[ \frac{\Omega_0}{1 - \sigma} (1 + z)^{(3+\sigma)} + \left(1 - \frac{\Omega_0}{1 - \sigma}\right) (1 + z)^{(2\sigma+2)} \right]. \quad (6)$$

Where,  $z (= \frac{1}{a} - 1)$ , is the redshift parameter.  $H_0$  denotes the present-day value of the Hubble parameter, and the density parameter  $\Omega_0$ , defined as,

$$\Omega_0 = \frac{\bar{\rho}_0}{\frac{3H_0^2}{8\pi G}},$$

originates from the present day background fluid density  $\bar{\rho}_0$ .

From (6), it is apparent that the density parameter and the equation of state parameter receive significant modification in the presence of  $\sigma$ . As  $\sigma$  appears in the fluid dynamical equations as NC correction term, it should follow the theoretical bound  $-3.0 < \sigma < 3.0$ . Since  $\frac{\Omega_0}{1-\sigma}$ , acts as an effective density parameter, and should always be positive. In an ideal fluid structure Hubble function deals with two fundamental degrees of freedom  $\Omega_0$  and  $H_0$ . In this modified model the NC correction term  $\sigma$  is also playing the role of a d.o.f.

## III. BACKGROUND COSMIC DYNAMICS

If NC correction term  $\sigma$  is set to zero in (6), we obtain a Hubble function

$$H^2 = H_0^2 \left[ \Omega_0 (1 + z)^3 + (1 - \Omega_0) (1 + z)^2 \right],$$

that includes contributions from matter and curvature sector. So, it is apparent that  $\sigma$  will bring a significant change in the evolution picture. We are going to check the effect of the inclusion of  $\sigma$  on the background cosmic dynamics.

To start with, we have discussed about deceleration parameter, defined as,

$$q = -1 - \frac{\dot{H}}{H^2}. \quad (7)$$

We have to analyze the effect of  $\sigma$  on the deceleration parameter. For this job, with the help of (1) and (6) we can deduce the modified deceleration parameter  $q(z)$ . The expression of modified  $q(z)$  will be,

$$q(z) = \sigma + \frac{1}{2} \frac{\Omega_0 (1 + z)^{(3+\sigma)}}{\left[ \frac{\Omega_0}{1 - \sigma} (1 + z)^{(3+\sigma)} + \left(1 - \frac{\Omega_0}{1 - \sigma}\right) (1 + z)^{(2\sigma+2)} \right]}. \quad (8)$$

The above expression (8) shows the evolution of deceleration parameter  $q(z)$  having significant information about late-time acceleration, which can be seen in Fig-1, where, we have investigated the nature of  $q(z)$  for a set of permissible  $\sigma$  values as discussed in the previous section, and for a proper theoretical choice of  $\Omega_0$ . We have observed that for  $\sigma > 0$ ,  $q(z) > 0$  at very early times (higher  $z$  values). We know that

$$q(z) = -\frac{\ddot{a}}{H^2 a},$$

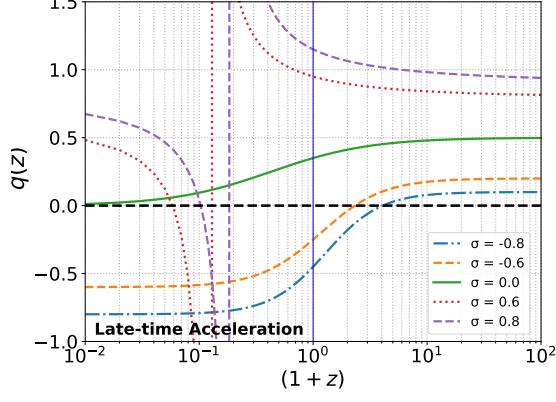


FIG. 1: The evolution of deceleration parameter  $q(z)$  for different choice of  $\sigma$ .

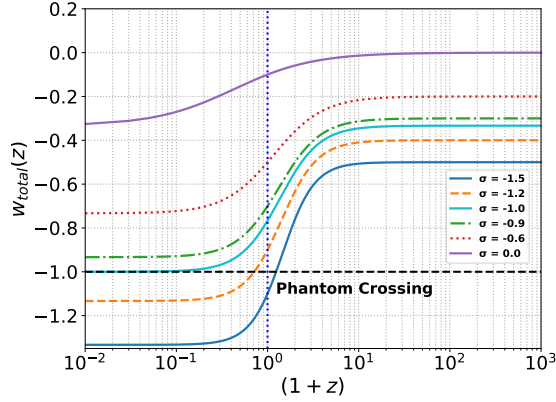


FIG. 2: The evolution of overall equation of state parameter for different choice of  $\sigma$ .

where  $H = \frac{\dot{a}}{a}$ , we can infer that for  $\sigma > 0$ , we get  $\ddot{a} < 0$ , which corresponds to a decelerating phase of cosmic expansion. However, this would be inconsistent with observational evidence. Moreover, in this case, the choice of  $\sigma > 0$  results in a discontinuity in  $q(z)$  in the  $z < 0$  region (i.e., in the future). This intriguing behavior could be interpreted as a potential 'singularity'. In the absence of  $\sigma$  (i.e.,  $\sigma = 0$ ), we also observe a phase of negative acceleration in both the early universe and at present. However, at very future times (i.e.,  $z < 0$ ), the acceleration tends to zero, which implies that the universe is approaching a static state. This suggests an interesting aspect of a static universe scenario.

The center of interest is the negative valued region of  $\sigma$ . In this case, we are achieving cosmic acceleration both at the present day and in the very future. This case has been visualized in Fig-1. We have also observed that more negative values of  $\sigma$  cause the entry of  $q(z)$  into the zone  $q(z) < 0$  at relatively higher redshift. Therefore, it is theoretically clear that in the negative valued region of  $\sigma$ , our model can explain cosmic acceleration.

We have also examined the behavior of the overall equation of state with respect to our model. We can define our overall equation of state,

$$w_{total} = -1 - \frac{2\dot{H}}{3H^2}. \quad (9)$$

From (6), we can provide the expression of the overall equation of state.

$$w_{total}(z) = -1 + \frac{1}{3} \frac{\left[ \frac{(3+\sigma)\Omega_0}{1-\sigma} (1+z)^{(3+\sigma)} + (2+2\sigma)\left(1 - \frac{\Omega_0}{1-\sigma}\right)(1+z)^{(2\sigma+2)} \right]}{\left[ \frac{\Omega_0}{1-\sigma} (1+z)^{(3+\sigma)} + \left(1 - \frac{\Omega_0}{1-\sigma}\right)(1+z)^{(2\sigma+2)} \right]} \quad (10)$$

The expression (10) highlights the behavior of the expansion dynamics of the universe based on our model. The additional term deviating from  $-1$  in (10) is generated from  $\dot{H}$ , which essentially represents the change in the expansion rate. As in the case of  $q(z)$ , we have also analyzed the evolution of the overall equation of state parameter  $w_{total}$  for different choices of  $\sigma$ . In the absence of  $\sigma$  (which means  $\sigma = 0$ ), we observed that  $w_{total}(z)$  approaches zero from higher redshift to  $z \sim 10$ . In the region of  $z < 10$ , we can observe that  $w_{total}(z)$  trends

towards entering the negative-valued zone, and this behavior is sustained in the future. Thus, in the absence of  $\sigma$ , we can see a transformation of  $w_{total}$  from a dust-like nature ( $w_{total} = 0$ ) to an expanding scenario ( $w_{total} < 0$ ). However, when the values of  $\sigma$  become negative, we observe the quintessential behavior of the cosmic expansion dynamics. An interesting fact here is that when  $\sigma$  is less than  $-1$ , we can find a phantom-like behavior, but this violates the theoretical bound on  $\sigma$ . Therefore, our model exhibits proper quintessence-like behavior in the

background cosmic dynamics. We have highlighted this fact in Fig-2.

#### IV. OBSERVATIONAL DATASET AND METHODOLOGY

In this section we highlight the observational datasets which have been used to investigate our model. We also mention the statistical methods for performing observational formalities.

So, our model has two fundamental degrees of freedom  $H_0$  and  $\Omega_0$  and one external degree of freedom  $\sigma$ . This external degree of freedom  $\sigma$  is the center of interest here, as it is the main theoretical input. We also need to include the observational flavor about  $\sigma$ .

The following dataset we have used for analysis.

- **OHD:** The most fundamental and primary dataset used to constrain cosmological models is the  $H(z)$  dataset. In this work, we utilize an updated collection of 57 data points of  $H(z)$ , which we refer to as OHD, as presented in [26]. Out of these 57 data points, 31 are derived from Cosmic Chronometer (CC) measurements, which involve the differential age (DA) between evolving galaxies, while the remaining 26 data points are obtained from Baryonic Acoustic Oscillations (BAO) measurements related to galaxy clustering phenomena.
- **SNeIa:** The following type Ia supernovae dataset which we have used for our analysis.
  1. **Union3:** The latest Union3 compilation includes 2087 SNeIa from 24 datasets, standardized to a consistent distance scale via SALT3 light curve fitting. These are analyzed and binned using the UNITY1.5 Bayesian framework, yielding 22 binned distance modulus measurements in the redshift range  $0.05 < z < 2.26$ , which we adopt in this article [27].
  2. **Pantheon+:** This type Ia Supernovae (SNeIa) data is an updated version of Pantheon sample. It includes 1701 light curve measurements from 1550 distinct supernovae. This sample is activated with in redshift range  $z = [0.001, 2.26]$  [28]. We have implemented here 1590 data points from this sample to demolish the effect of peculiar velocity issues [29].
- **DESI:** The Dark Energy Spectroscopic Instrument (DESI) data includes both isotropic and anisotropic Baryonic Acoustic Oscillations (BAO) measurements, which are based on BAO matter clustering as a standard ruler. For isotropic BAO measurements, the angle-averaged distance rescaled by the co-moving sound horizon ( $r_d$ ) at the drag epoch,  $D_V(z)/r_d$ , plays a key role. In contrast, anisotropic BAO measurements are represented by  $D_M(z)/r_d$

Parameters	Priors
$H_0$	[50, 100]
$\Omega_0$	[0, 1]
$\sigma$	[-2.9, 0.9]

TABLE I: Priors on cosmological parameters are constrained using the observational datasets discussed.

and  $D_H(z)/r_d$ , where  $D_M$  denotes the co-moving distance and  $D_H$  refers to the Hubble horizon distance. For this study, we have utilized data from DESI Data Release I, which includes tracers from the Bright Galaxy Sample (BGS), Luminous Red Galaxies (LRG), Emission Line Galaxies (ELG), Quasars (QSO), and the Lyman- $\alpha$  forest. The complete DESI dataset used in this work is presented in Table I of [30].

We have utilized the Markov Chain Monte Carlo (MCMC) method to constrain our model using the observational datasets mentioned above. For this purpose, we have utilized the publicly available Python-based package `emcee`<sup>2</sup> [31]. The `emcee` sampler efficiently explores the posterior distribution in high-dimensional spaces by using an ensemble of walkers. We marginalize the likelihood across the datasets with priors for the free parameters, as specified in Table I. Additionally, we used the `getdist` package<sup>3</sup> [32] to analyze our MCMC chains, ensuring the proper physical interpretation of our cosmological parameters [32].

#### V. RESULTS

In this section, we will provide a comprehensive discussion of the overall results from our analysis, focusing on key findings and their implications. We have examined the observational constraints within  $1-\sigma$  uncertainties, and the results for different data sets are presented in Table-II. These constraints are crucial for evaluating the accuracy and reliability of our model, as they reflect the range of values that are statistically consistent with the observed data.

First, we analyze the Hubble parameter in the context of our model and compare it with the  $\Lambda$ CDM model in Fig-3, using standard values for essential cosmological parameters. In the low redshift region, the evolution of our model is nearly indistinguishable from that of  $\Lambda$ CDM. However, at higher redshifts, our model exhibits a noticeable and sustained deviation.

First, we will discuss the observational constraints related to the outcome of the Hubble Data Mission (OHD).

<sup>2</sup> <https://github.com/dfm/emcee>

<sup>3</sup> <https://github.com/cmbant/getdist>

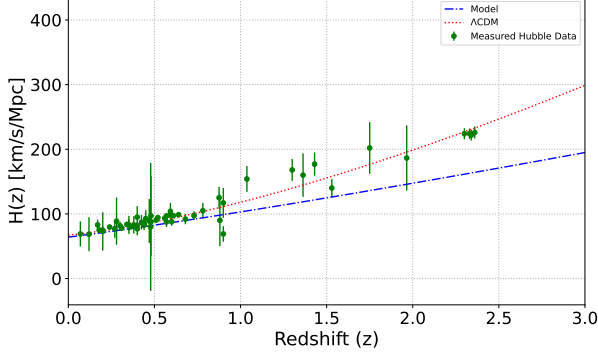


FIG. 3: Compariosn of Hubble parameter evolution with  $\Lambda$ CDM against the observational data(OHD).

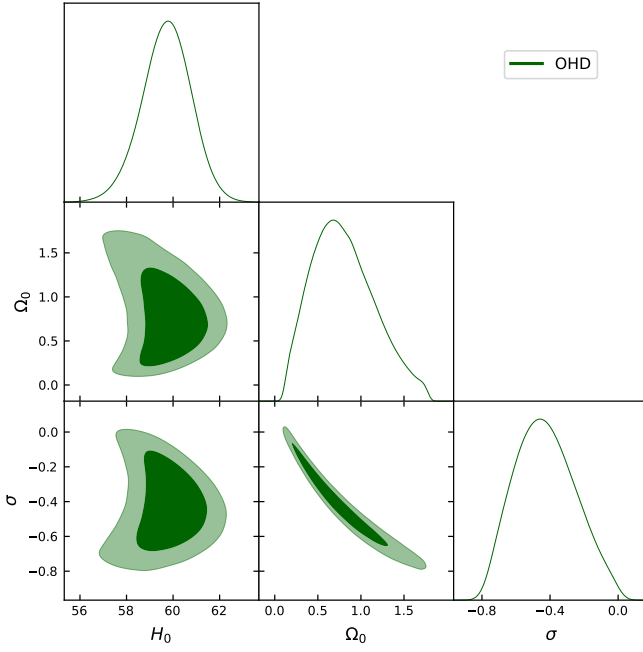


FIG. 4: 1D posterior distribution with 2D contour presentation for our model only for OHD dataset

Looking at  $H_0$ , we observe that the value obtained from the Hubble Data Mission (OHD) is lower. We found that  $H_0 = 59.7^{+1.1}_{-0.98}$ , which is not a suitable value for  $H_0$ . From the OHD data alone, we obtained  $\Omega_0 = 0.80^{+0.28}_{-0.45}$ . The model parameter  $\sigma$  has been constrained in the negative-valued region ( $\sigma = -0.42^{+0.16}_{-0.20}$ ). We also provide the 2D contour presentation in Fig-4.

We observed a preferred negative correlation between  $\sigma$  and  $\Omega_0$ , but the correlations in the  $\Omega_0 - H_0$  and  $\sigma - H_0$  planes are not sufficiently clear to draw definitive conclusions. So we are motivated now for adding some other missions for analysis.

Before implementing further missions in our MCMC analysis, we also show the evolution of the distance mod-

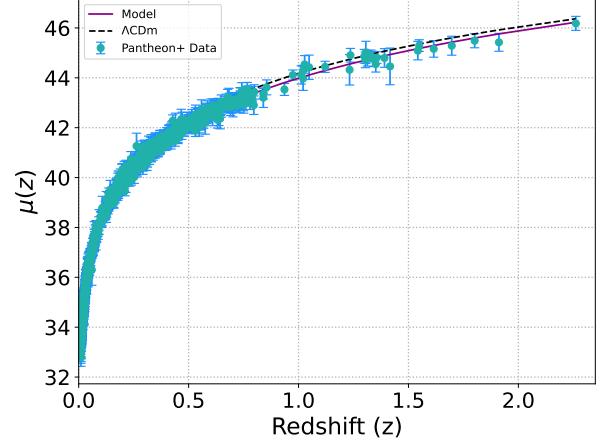


FIG. 5: The evolution of distance modulus with redshift and it is compared to  $\Lambda$ CDM and Pantheon+ dataset

ulus  $\mu(z)$  for our model, along with a comparison to  $\Lambda$ CDM, using the latest Pantheon+ dataset. This is presented in Fig-5.

First, we encountered this through the above-mentioned type Ia supernovae (SNeIa) missions with OHD. However, with the inclusion of Pantheon+, we observed a significant improvement in the  $H_0$  measurements. For the combined OHD+Pantheon+ data, we obtained  $H_0 = 73.03 \pm 0.19$ , which is very close to the local measurements of  $H_0$  [33]. With OHD+DESI+Pantheon+ we have obtained  $H_0 = 72.27 \pm 0.17$ .

For the other SNeIa case (Union3), the constrained value of  $H_0$  is comparatively lower than the Planck-based measurements [34].

The parameter  $\Omega_0$  may resemble a matter density parameter, and regarding  $\Omega_0$ , we observed that its value is larger. However, it is rescaled by  $(1 - \sigma)$  here. Therefore, the large value of  $\Omega_0$  is not a cause for concern in this context. Since  $\Omega_0$  is a cosmic parameter, the rescaled quantity  $\frac{\Omega_0}{(1 - \sigma)}$  can act like an effective density parameter. The addition of DESI, along with the corresponding SNeIa, causes the  $\Omega_0$  values to decrease slightly.

Compared to the other supernova datasets, Pantheon+ improves the 1- $\sigma$  uncertainties. The  $\sigma$  value for Pantheon+ is lower than the case of Union3, which is the opposite of what is observed for  $H_0$ . This fact is also highlighted in the 2D contour presentation in Fig-7.  $\sigma$  is negatively correlated with both  $H_0$  and  $\Omega_0$ , but the negative correlation is stronger in the  $\sigma - \Omega_0$  plane. The addition of DESI with two different OHD+SNeIa missions also maintains the same correlation properties. DESI has improved the 1- $\sigma$  uncertainties, and the 2D contour area is smaller in the case of the OHD+DESI+SNeIa missions. This reflects the strong constraining power of DESI.

We have also discussed cosmic acceleration in several of our conversations, focusing on the observational per-



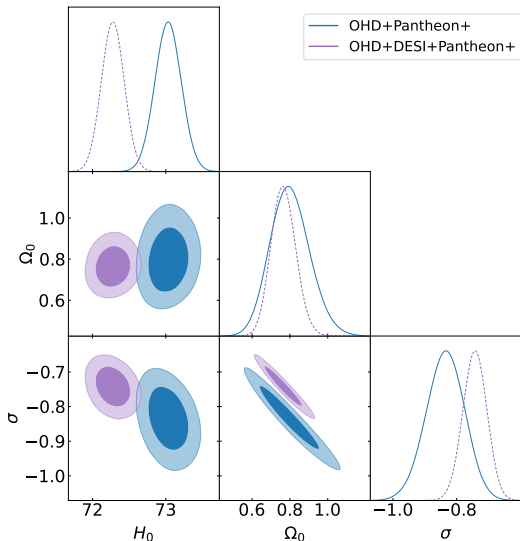


FIG. 6: 2D contour plots with 1D posterior distribution for OHD+Pantheon+ and OHD+DESI+Pantheon+

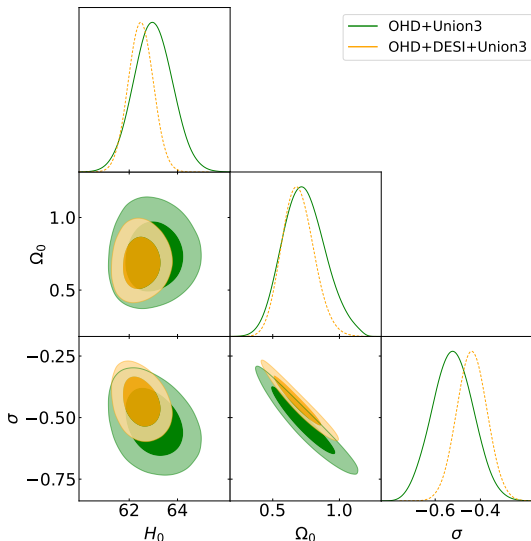


FIG. 7: 2D contour plots with 1D posterior distribution for OHD+Union3 and OHD+DESI+Union3 combination.

spective. Specifically, we examined the nature of acceleration through the evolution of the deceleration parameter, based on observational constraints. This is presented in Fig. 8. We have observed that the addition of DESI, along with the relative SNeIa, leads to a decrease in the present-day acceleration. Figure 8 actually shows this effect. In the case of Pantheon+, it has been observed that the accelerating phase began slightly earlier compared to

Union3.

We have also derived the 2D contour for the overall equation of state  $w_{total}$  based on the observational constraints of OHD+Pantheon+, OHD+Union3, OHD+DESI+Union3 and OHD+DESI+Pantheon+. This is presented in Fig-9. From the 2D contour of  $w_0 - \Omega_0$  and  $w_0 - \sigma$ , it is clear that our model exhibits quintessence-like behavior in the context of cosmic acceleration. In all the cases,  $w_0$  is negatively correlated with  $\Omega_0$  and it has a positive correlation with model parameter  $\sigma$ .

## VI. MODEL COMPARISON WITH INFORMATION CRITERION

We have derived a generalized model based on Newtonian cosmology with a non-commutative term and completed the essential cosmological formalities related to it. Consequently, it is important to assess the fitting strength and statistical quality of the model. To evaluate these qualities, we have adopted the Akaike Information Criterion (AIC) [35] and the Bayesian Information Criterion (BIC) [36].

The AIC is derived from Kullback-Leibler (KL) information theory, which is based on the principle of minimizing KL divergence. KL divergence is a measure of relative entropy used to compare two probability distributions. In this context, it compares the model distribution and the data distribution being fitted [37]. The AIC is defined as:

$$\text{AIC} \equiv -2 \ln \mathcal{L}_{\max} + 2k \quad (11)$$

where  $\mathcal{L}_{\max}$  denotes the maximum likelihood, and  $k$  is the number of degrees of freedom in the model.

BIC is the Gaussian approximation of the Bayesian evidence (BE) [37], and serves as an estimator for BE in this case. It is defined as:

$$\text{BIC} \equiv -2 \ln \mathcal{L}_{\max} + k \ln N \quad (12)$$

where  $N$  is the number of data points. The maximum likelihood, denoted as  $\mathcal{L}_{\max}$ , is determined by  $\mathcal{L}_{\max} = \mathcal{L}_{\max}(\theta_{\max})$ , where  $\theta_{\max}$  represents the set of observational constraints on the cosmological parameters obtained from MCMC.

The primary objective of this work is to compare our model with an established reference model, specifically the vanilla  $\Lambda$ CDM model. To facilitate this comparison, we introduce the quantities  $\Delta\text{AIC}$  and  $\Delta\text{BIC}$ , which are defined as follows:

$$\Delta\text{AIC} = \text{AIC}_{\text{model}} - \text{AIC}_{\Lambda\text{CDM}}$$

and

$$\Delta\text{BIC} = \text{BIC}_{\text{model}} - \text{BIC}_{\Lambda\text{CDM}}.$$

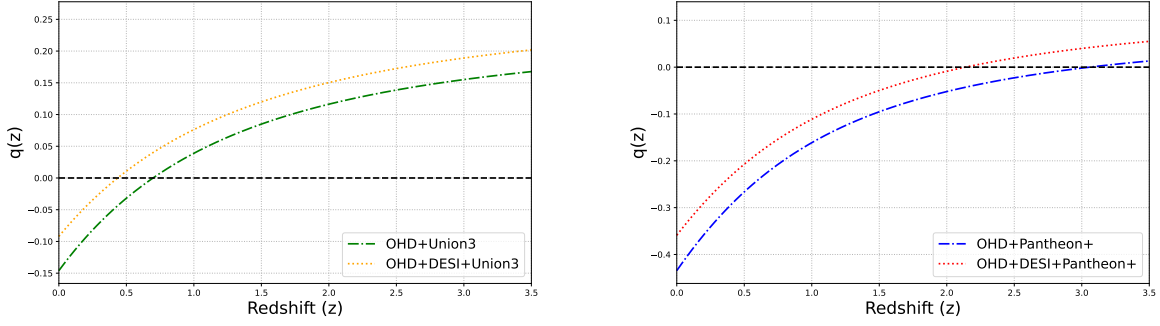


FIG. 8: The evolution of  $q(z)$  on the basis of observational constraints of OHD+SNeIa and OHD+DESI+SNeIa datasets

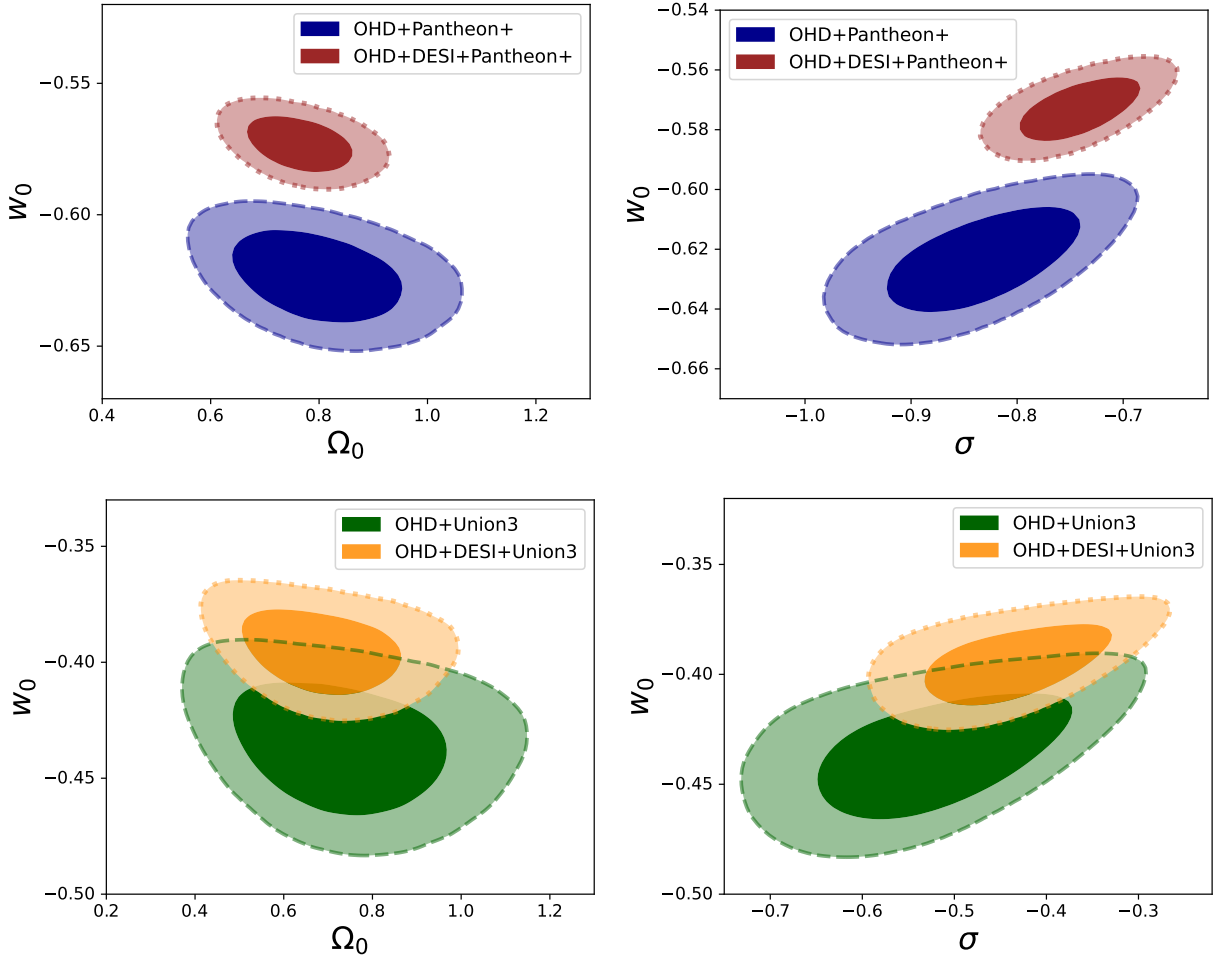


FIG. 9: The derived 2D contour of the present-day overall equation of state parameter based on the observational constraints from OHD+SNeIa and OHD+DESI+SNeIa missions.

We know that  $\chi^2$  is defined as  $\chi^2 = -2 \ln \mathcal{L}_{\max}$ . We also adopt the change in  $\chi^2$  as  $\Delta\chi^2 = \chi^2_{\text{model}} - \chi^2_{\Lambda\text{CDM}}$ . We have also estimated  $\text{AIC}_{\Lambda\text{CDM}}$ ,  $\text{BIC}_{\Lambda\text{CDM}}$ , and  $\chi^2_{\Lambda\text{CDM}}$  for all the dataset combinations we used.

Based on Table-III and Table-IV, we discuss the statistical compatibility of our model with respect to the  $\Lambda\text{CDM}$  reference model. We have adopted all the relevant information for  $\Delta\text{AIC}$  and  $\Delta\text{BIC}$  presented in Table-III

Dataset	$H_0$	$\Omega_0$	$\sigma$
OHD	$59.7^{+1.1}_{-0.98}$	$0.80^{+0.28}_{-0.45}$	$-0.42^{+0.16}_{-0.20}$
OHD+Union3	$63.00 \pm 0.81$	$0.74^{+0.15}_{-0.17}$	$-0.521 \pm 0.091$
OHD+Pantheon+	$73.03 \pm 0.19$	$0.801^{+0.096}_{-0.11}$	$-0.835 \pm 0.063$
OHD+DESI+Union3	$62.48 \pm 0.54$	$0.69^{+0.11}_{-0.13}$	$-0.437 \pm 0.067$
OHD+DESI+Pantheon+	$72.27 \pm 0.17$	$0.766 \pm 0.066$	$-0.742 \pm 0.041$

TABLE II: Details of Observational Constraints with in  $1\text{-}\sigma$  uncertainties.

$\Delta\text{AIC}$	Level of support to model
$< 2$ (including $< 0$ )	Significant support
Between 4 and 7	Considerably less support for the model
Greater than 10	Essentially no support for the model

TABLE III: The role of  $\Delta\text{AIC}$  in evaluating the level of support for a specific model.

$\Delta\text{BIC}$	Evidence against
Less than 2	No evidence
Between 2 and 6	Mild to positive
Between 6 and 10	Strong
Greater than 10	Very Strong

TABLE IV: The significance of  $\Delta\text{BIC}$  as evidence that contradicts a model.

and Table-IV from [38, 39].

Finally, We have computed the AIC and the BIC for our model. Additionally, we have included a comparison of our model with the  $\Lambda\text{CDM}$  model, which serves as the reference model in this analysis. All the related information has been provided in Table-V.

According to the references in Table III and Table IV, our model is preferred, with significance observed only in the case of OHD+Union3. There is comparatively less support for our model in the case of the OHD mission alone. However, in all other cases, including Pantheon and DESI, the  $\Lambda\text{CDM}$  model receives the most support.

## VII. SUMMARY AND CONCLUSIONS

The model presented in (6) focuses on the external degrees of freedom, represented by the parameter  $\sigma$ . This parameter originates from the extended NC fluid term and plays a crucial role in cosmology. It eliminates the need for a cosmological constant or any other dark energy fluid in this scenario. This has been verified from both theoretical and observational perspectives, with the theoretical bound of  $\sigma$  being satisfied by the observational analysis. Therefore, it can be considered as an alternative approach, drawing attention to the concept of matter creation cosmology.

Although all our analysis is based on background cosmology, it can be extended to a perturbative scenario. By including the perturbative scenario, one can gain further physical insight into the parameter  $\sigma$ . This approach can also be interpreted in the context of CMB-based observations.

Finally, we aimed to establish a connection showing that the extended NC fluid can also fulfil the requirements of matter creation cosmology. In our approach, we have demonstrated that late-time acceleration can be explained without invoking terms such as the cosmological constant. The extended non-commutative fluid can alternatively mimic the creation of cold dark matter phenomena.

## VIII. ACKNOWLEDGMENT

We are thankful to Prof. Subir Ghosh from ISI, Kolkata, Prof. Supriya Pan from Presidency University, Kolkata and Dr Souvik Ghose from HRI, Allahabad, for their helpful discussions. Raj Kumar Das is also thankful to Rahul Shah from ISI, Kolkata, for some helpful discussions. We thank ARIES and Presidency University for providing the necessary computational facility.



Dataset	Model	AIC	$\Delta$ AIC	BIC	$\Delta$ BIC	$\chi^2$	$\Delta\chi^2$
OHD	$\Lambda$ CDM	48.09	0	58.91	0	44.09	0
	Model1	54.46	6.39	70.70	11.79	48.46	4.39
OHD+Pantheon+	$\Lambda$ CDM	1516.80	0	1527.61	0	1512.80	0
	Model1	1619.83	103	1636.05	108.44	1613.83	101
OHD+DESI+Pantheon+	$\Lambda$ CDM	1561.69	0	1572.52	0	1557.69	0
	Model1	1855.81	294.12	1872.05	299.48	1849.81	292.12
OHD+Union3	$\Lambda$ CDM	105.51	0	110.53	0	101.51	0
	Model1	104.65	-0.86	111.76	1.23	98.65	-2.86
OHD+DESI+Union3	$\Lambda$ CDM	100.82	0	105.84	0	96.82	0
	Model1	155.45	54.63	162.98	57.14	149.45	52.63

TABLE V: Comparison of AIC,  $\Delta$ AIC, BIC,  $\Delta$ BIC, and  $\chi^2$  for models ( $\Lambda$ CDM and Model) across multiple datasets.

- 
- [1] A. G. Riess *et al.* (Supernova Search Team), *Astron. J.* **116**, 1009 (1998), [arXiv:astro-ph/9805201](#).
- [2] S. Perlmutter *et al.* (Supernova Cosmology Project), *Astrophys. J.* **517**, 565 (1999), [arXiv:astro-ph/9812133](#).
- [3] J. Sola, J.Phys.Conf.Ser. (2013), [arXiv:1306.1527 \[astro-ph.CO\]](#).
- [4] S. Pan and W. Yang, *Springer Series in Astrophysics and Cosmology*, 531 (2023), [arXiv:2310.07260 \[astro-ph.CO\]](#).
- [5] L. A. Anchordoqui, E. Di Valentino, S. Pan, and W. Yang, *Journal of High Energy Astrophysics* **32**, 28–64 (2021).
- [6] E. Di Valentino, O. Mena, S. Pan, L. Visinelli, W. Yang, A. Melchiorri, D. F. Mota, A. G. Riess, and J. Silk, *Class. Quant. Grav.* **38**, 153001 (2021), [arXiv:2103.01183 \[astro-ph.CO\]](#).
- [7] E. Di Valentino, S. Pan, W. Yang, and L. A. Anchordoqui, *Phys. Rev. D* **103**, 123527 (2021), [arXiv:2102.05641 \[astro-ph.CO\]](#).
- [8] L. A. Anchordoqui, E. Di Valentino, S. Pan, and W. Yang, *JHEAp* **32**, 28 (2021), [arXiv:2107.13932 \[astro-ph.CO\]](#).
- [9] X. Li and A. Shafieloo, *Astrophys. J. Lett.* **883**, L3 (2019), [arXiv:1906.08275 \[astro-ph.CO\]](#).
- [10] W. Yang, E. Di Valentino, S. Pan, A. Shafieloo, and X. Li, *Phys. Rev. D* **104**, 063521 (2021), [arXiv:2103.03815 \[astro-ph.CO\]](#).
- [11] I. Zlatev, L.-M. Wang, and P. J. Steinhardt, *Phys. Rev. Lett.* **82**, 896 (1999), [arXiv:astro-ph/9807002](#).
- [12] S. Weinberg, *Rev. Mod. Phys.* **61**, 1 (1989).
- [13] G. Steigman, R. C. Santos, and J. A. S. Lima, *JCAP* **06**, 033 (2009), [arXiv:0812.3912 \[astro-ph\]](#).
- [14] J. A. S. Lima, J. F. Jesus, and F. A. Oliveira, *JCAP* **11**, 027 (2010), [arXiv:0911.5727 \[astro-ph.CO\]](#).
- [15] J. A. S. Lima, R. C. Santos, and J. V. Cunha, *JCAP* **03**, 027 (2016), [arXiv:1508.07263 \[gr-qc\]](#).
- [16] S. Basilakos and J. A. S. Lima, *Phys. Rev. D* **82**, 023504 (2010), [arXiv:1003.5754 \[astro-ph.CO\]](#).
- [17] J. S. Alcaniz and J. A. S. Lima, *Astron. Astrophys.* **349**, 729 (1999), [arXiv:astro-ph/9906410](#).
- [18] M. P. Freaza, R. S. de Souza, and I. Waga, *Phys. Rev. D* **66**, 103502 (2002).
- [19] S. Halder, J. de Haro, S. Pan, T. Saha, and S. Chakraborty, (2025), [arXiv:2502.03256 \[gr-qc\]](#).
- [20] W. Zimdahl, D. J. Schwarz, A. B. Balakin, and D. Pavon, *Phys. Rev. D* **64**, 063501 (2001), [arXiv:astro-ph/0009353](#).
- [21] P. Das and S. Ghosh, *Eur. Phys. J. C* **76**, 627 (2016), [Erratum: *Eur.Phys.J.C* 77, 64 (2017)], [arXiv:1601.01430 \[hep-th\]](#).
- [22] P. Das and S. Ghosh, *Phys. Rev. D* **96**, 111901 (2017), [arXiv:1707.03153 \[hep-th\]](#).
- [23] P. Das and S. Ghosh, *Phys. Rev. D* **98**, 084047 (2018), [arXiv:1804.07475 \[hep-th\]](#).
- [24] Y.-J. Ren and K. Ma, *Int. J. Mod. Phys. A* **33**, 1850093 (2018), [arXiv:1802.10452 \[physics.gen-ph\]](#).
- [25] A. K. Mitra, R. Banerjee, and S. Ghosh, *JCAP* **10**, 057 (2018), [arXiv:1804.10404 \[hep-th\]](#).
- [26] A. Bouali, H. Chaudhary, R. Hama, T. Harko, S. V. Sabau, and M. S. Martín, *Eur. Phys. J. C* **83**, 121 (2023), [arXiv:2301.10278 \[gr-qc\]](#).
- [27] D. Rubin *et al.*, (2023), [arXiv:2311.12098 \[astro-ph.CO\]](#).
- [28] D. Brout *et al.*, *Astrophys. J.* **938**, 110 (2022), [arXiv:2202.04077 \[astro-ph.CO\]](#).
- [29] C.-G. Park, J. de Cruz Pérez, and B. Ratra, *Phys. Rev. D* **110**, 123533 (2024), [arXiv:2405.00502 \[astro-ph.CO\]](#).
- [30] A. G. Adame *et al.* (DESI), *JCAP* **02**, 021 (2025), [arXiv:2404.03002 \[astro-ph.CO\]](#).
- [31] D. Foreman-Mackey, D. W. Hogg, D. Lang, and J. Goodman, *Publ. Astron. Soc. Pac.* **125**, 306 (2013), [arXiv:1202.3665 \[astro-ph.IM\]](#).
- [32] A. Lewis, (2019), [arXiv:1910.13970 \[astro-ph.IM\]](#).
- [33] A. G. Riess *et al.*, *Astrophys. J. Lett.* **934**, L7 (2022), [arXiv:2112.04510 \[astro-ph.CO\]](#).
- [34] N. Aghanim *et al.* (Planck), *Astron. Astrophys.* **641**, A6 (2020), [Erratum: *Astron.Astrophys.* 652, C4 (2021)], [arXiv:1807.06209 \[astro-ph.CO\]](#).
- [35] H. Akaike, *IEEE Trans. Automatic Control* **19**, 716 (1974).
- [36] G. Schwarz, *Annals Statist.* **6**, 461 (1978).
- [37] R. Trotta, *Contemp. Phys.* **49**, 71 (2008), [arXiv:0803.4089 \[astro-ph\]](#).
- [38] M. Rezaei, S. Pan, W. Yang, and D. F. Mota, *JCAP* **01**, 052 (2024), [arXiv:2305.18544 \[astro-ph.CO\]](#).
- [39] M. Rezaei, M. Malekjani, and J. Sola, *Phys. Rev. D* **100**, 023539 (2019), [arXiv:1905.00100 \[gr-qc\]](#).